Journal of Engineering and Technology for Industrial Applications

ISSN ONLINE: 2447-0228

ITEGAM-JETIA

Manaus, v.12 n.58, p. 1-10. March/April, 2026.
DOI: https://doi.org/10.5935/jetia. v12i58.2064

RESEARCH ARTICLE OPEN ACCESS

COMPACT SPIRAL TRANSFORMER DESIGN FOR HIGH-EFFICIENCY INTERLEAVED FLYBACK CONVERTERS IN SOLAR POWER SYSTEMS

Benzidane Mohammed Ridha[1], Namoune Abdelhadi[2], Benbouzid Zineb[3], Benyamina Mansour[4], Meskine Said[5]

[1, 2, 3, 4, 5]Elaboration and Characterization Physico-Mechanical and Metallurgical of Materials Laboratory (ECP3M) Abdelhamid Ibn Badis University of Mostaganem, Mostaganem, Algeria.

[1]https://orcid.org/0000-0003-1761-4618, [2]https://orcid.org/0000-0001-9017-065X, [3]https://orcid.org/0000-0002-5531-7705, [4]https://orcid.org/0000-0002-8424-5296, [5]https://orcid.org/0000-0002-3922-6619

Email: *ridha.benzidane@univ-mosta.dz

ARTICLE INFO

Article History
Received: May 5, 2025
Reviewed: January 30, 2026
Accepted: February 6, 2026
Published: March 31, 2026

Keywords:
Flyback converters,
HIGH-EFFICIENCY,
Planar coil,
COMPACT TRANSFORMER,
Solar system.

ABSTRACT

This paper explores the design, modeling, and optimization of a spiral transformer integrated into an interleaved flyback converter tailored for photovoltaic (PV) applications. The transformer features two square planar spiral coils with an outer diameter of 9000 µm and an inner diameter of 6000 µm, yielding primary and secondary inductances of 0.128 µH and 0.226 µH, respectively, at a 5 MHz operating frequency. The miniaturized design includes 3 primary turns and 4 secondary turns, with conductor widths of 500 µm and 300 µm, respectively. An electrical model accounts for parasitic effects, such as series resistances (0.195 Ω for primary, 0.282 Ω for secondary) and capacitances (inter-turn and oxide layer), which are minimized to boost efficiency. Frequency-dependent behavior is analyzed using MATLAB, identifying a resonance frequency of 20 MHz and a coupling coefficient of 0.87. The interleaved flyback converter, simulated in PSIM, delivers a stable 48 V output voltage and 3.2 A output current from a 162 W input, achieving 95% efficiency. This work validates the potential of compact, high-efficiency transformers for advancing PV energy conversion systems.

I. INTRODUCTION

Interleaved Flyback converters, incorporating miniaturized transformers, are versatile and find application in various sectors such as solar energy, wireless chargers, and electric vehicle equipment [1], [2]. Compact and efficient, they are favored for their suitability in environments where space and energy efficiency matter [3], [4]. The miniaturization of photovoltaic converters offers significant advantages: improved energy efficiency, reduced foot print, increased power density, and enhanced integration into complex systems [4], [5]. These advancements facilitate the accessibility and adaptability of solar energy for various applications [6], [7].

However, the miniaturization of flyback converters involves that of their transformers, there by requiring the reduction of coil dimensions [8], [9]. These coils necessitate sophisticated technological advancements, particularly in high-flux-density magnetic materials, to increase energy density and minimize losses [10], [11].Planar spiral coils are studied for their potential for miniaturization and electronic versatility. Research focuses on optimizing their design, materials, and manufacturing techniques to meet the requirements of compactness and integration into advanced systems [12], [13].

In this study, we present the geometric dimensioning of a transformer consisting of two square planar spiral coils. This transformer plays a crucial role within a flyback converter specifically designed for a photovoltaic system. Our main objective in this geometric design is to reduce the transformer size while minimizing energy losses. These efforts align with the specific requirements outlined in the flyback converter's specifications. The geometric dimensioning process is meticulously conducted, taking into account the converter's specifications. Our aim is to define the values of geometric parameters to subsequently calculate the technological parameters. This will ensure that parasitic effects are maintained at a negligible level, thereby ensuring optimal efficiency of the transformer.

In addition to the geometric sizing step, we undertake an in-depth study of the impact of frequency on various transformer parameters, namely, the inductances of the primary and secondary coils, their series resistances, as well as the quality factors and the coupling coefficient. This study will determine the sensitivity of the transformer at different frequencies. To validate our approach, we will conduct comprehensive simulations of the voltages and currents involved in the converter's operation. These simulations will confirm the proper functioning of the transformer integrated into the flyback converter, there by guaranteeing its efficiency and overall performances.

II. PRESENTATION OF INTERLEAVED FLYBACK CONVERTER

The interleaved flyback converter is used in the photovoltaic system in order to reduce the input current and increase the output power, as it includes two equal flyback converters connected in parallel and each of them includes the following components: the transformer, power electronic switch and diode, but they share the source *Vin* and capacitance *Cout* as shown in Figure 1. When operated, the phase between the two switches is set at 180 degrees.

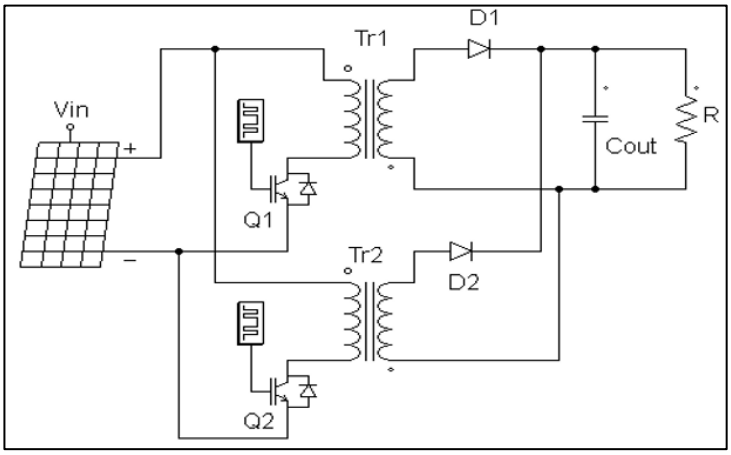

Figure 1: Schematic of an interleaved flyback converter.
Source: Authors, (2026).

To evaluate this type of DC/DC converter in a micro solar system, the spiral transformer will be studied when integrated into an interleaved flyback converter enhanced with the following specification: Input voltage, Vin = 24 [V]. Input power, Pin = 162 [W]. Output voltage, Vout = 48 [V]. Energy efficiency, η = 95%. Operating frequency, f = 5 [MHz], α = 0,6. Since the two micro transformers are equal, the primary inductances Lp of the micro transformers are calculated by the relation (1):

$$L_p = \frac{V_{in}^2 * \alpha^2}{2P_{in} * f} = 0{,}128\ [\mu H] \tag{1}$$

The turns ratio for the micro transformers (m) is calculated by the equation (2).

$$m = \frac{V_{out}}{V_{in}} * \frac{(1-\alpha)}{\alpha} = 1{,}33 \tag{2}$$

Using equation (3) the secondary inductances Ls of the micro transformers are calculated.

$$L_s = m^2 * L_p = 0{,}2264\ [\mu H] \tag{3}$$

The load resistance is calculated according to equation (4):

$$R = \frac{V_{out}^2}{P_{in} * \eta} = 14{,}97\ [\Omega] \tag{4}$$

The output voltage ripple ΔVout/Vout is estimated at 1%. By means of relation (5), the value of the output capacitor Cout is extracted:

$$C_{out} = \frac{\alpha}{\left(\frac{\Delta V_{out}}{V_{out}}\right) * R * f} = 0{,}8016\ [\mu F] \tag{5}$$

III. DIMENSIONING OF THE SQUARE COILS SPIRAL TRANSFORMER

Geometrically, the spiral transformer with square shape of windings is described by the parameters shown in Figure 2 as follows: do and di are the outer and inner diameter, tp and ts are the thickness of primary and secondary coils, Np and Ns are the number turns of primary and secondary coils, Wp, Sp, Ws and Ss are the width and spacing of adjacent turns of primary and secondary coils.

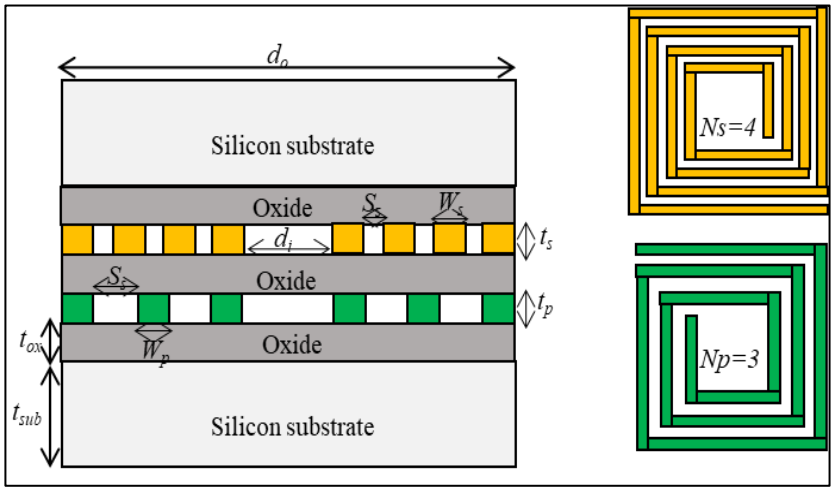

Figure 2: Geometric parameters of micro transformer spiral coils.
Source: Authors, (2026).

From the literature publications, there are several methods to calculate the inductance value. By choosing Wheeler method, the primary and secondary inductances of the transformer are expressed in the relations (6) and (7) [14], [15].

$$L_p = \frac{k_1 * \mu_0 * \left(\frac{d_o + d_i}{2}\right) * N_p^2}{1 + k_2 * \left(\frac{d_o - d_i}{d_o + d_i}\right)} \tag{6}$$

$$L_s = \frac{k_1 * \mu_0 * \left(\frac{d_o + d_i}{2}\right) * N_s^2}{1 + k_2 * \left(\frac{d_o - d_i}{d_o + d_i}\right)} \tag{7}$$

The coefficients k_1 and k_2 depend on geometrical structure of two coils. For the square geometry: $k_1 = 2.34$, $k_2 = 2.75$. To calculate all the geometrical parameters, we set the outer and inner diameters of the primary and secondary windings, respectively: $do = 9000$ [µm], $di = 6000$ [µm]. Based on relations (6) and (7), we extract the number of primary and secondary turns of the transformer as follows: $Np = 3$, $Ns = 4$. To determine the conductor thickness for each of the two inductors, the following condition must be met: $t_p = t_s \leq 2\delta$. Where δ is the skin thickness and is expressed as (8) [16]:

$$\delta = \sqrt{\frac{\rho_{Cu}}{\pi * \mu * f}} = 29{,}36\ [\mu m] \tag{8}$$

The width of individual winding W of both the primary and secondary windings of the transformer are calculated using relations (9) and (10) [17]. Where, the constant pitch P is the sum of the width of single turn and the distance between it and the next turn. We have chosen pitch values P for the primary and secondary coils respectively: $P_p = 600$ [µm], $P_s = 400$ [µm]

$$W_p = \frac{d_o - d_i - 2(N_p - 1) * P_p}{2} = 300\ [\mu m] \tag{9}$$

$$W_s = \left(\frac{d_o - d_i}{2}\right) - (N_s - 1) * P_s = 300\ [\mu m] \tag{10}$$

Also to calculate the distance S between adjacent coils of the two inductors of transformer, the relations (11) and (12) are used:

$$S_p = P_p - W_p = 300\ [\mu m] \tag{11}$$

$$S_s = P_s - W_s = 100\ [\mu m] \tag{12}$$

The expression used to calculate the conductor length of the primary and secondary windings of a transformer is given by (13) and (14) [18]:

$$l_p = 2 * N_p * \left[2 * d_i + \left(4 * N_p - 1\right) * W_p\right] = 86{,}4\ [mm] \tag{13}$$

$$l_s = 2 * N_s * [2 * d_i + (4 * N_s - 1) * W_s] = 124{,}8\ [mm] \tag{14}$$

All geometric dimension values of the tapered spiral transformer obtained after calculation are summarized in Table 1.

Table 1: Geometric dimension values of the tapered spiral transformer.

Geometric parameters	Primary coil		Secondary coil	
	Symbol	Values [µm]	Symbol	Values [µm]
Outer diameter	*do*	9000	*do*	9000
Inner diameter	*di*	6000	*di*	6000
Number of turns	*Np*	3	*Ns*	4
Width of conductor	*Wp*	300	*Ws*	300
Thickness of conductor	*tp*	58	*ts*	58
Spacing between turns	*Sp*	300	*Ss*	100
Length of conductor	*lp*	86400	*ls*	124800

Source: Authors, (2026).

IV. ELECTRICAL PARAMETER OF THE SQUARE COILS SPIRAL TRANSFORMER

Based on the physical model of Yue and Yong [19], the equivalent electrical circuit of a square coils spiral transformer is derived which shows all the parasitic effects when integrated into silicon. At high frequencies, the inductor is represented by three passives components where the series inductance *Ls* is related to the series resistance *Rs* and both are related to the capacitance series *Cs* of the inductor in parallel. Losses in the dielectric layer are represented by parasitic capacitance *Cox*. Substrate losses are represented by resistance and capacitance in silicon *Rsub, Csub*. *Cc* is the coupling capacitance between the primary and secondary windings of the transformer. According to the integrated spiral transformer in Figure 3, the expressions analytical for all electrical parameters of the equivalent circuit model are also given below [20], [21]:

$$C_c = \frac{d_o^2 * \varepsilon_{ox}}{t_{ox}} \tag{15}$$

$$R_{s-p} = \frac{\rho * l_p}{\delta\left(1-e^{-\left(\frac{t_p}{\delta}\right)}\right) * W_p} \quad , \quad R_{s-s} = \frac{\rho * l_s}{\delta\left(1-e^{-\left(\frac{t_s}{\delta}\right)}\right) * W_s} \tag{16}$$

$$C_{s-p} = \frac{t_p * l_p * \varepsilon_{ox}}{2 * S_p} \quad , \quad C_{s-s} = \frac{t_s * l_s * \varepsilon_{ox}}{2 * S_s} \tag{17}$$

$$C_{ox-p} = \frac{\varepsilon_{ox} * l_p * W_p}{2 t_{ox}} \quad , \quad C_{ox-s} = \frac{\varepsilon_{ox} * l_s * W_s}{2 t_{ox}} \tag{18}$$

$$C_{sub-p} = \frac{\varepsilon_{sub} * l_p * W_p}{2 t_{sub}} \quad , \quad C_{sub-s} = \frac{\varepsilon_{sub} * l_s * W_s}{2 t_{sub}} \tag{19}$$

$$R_{sub-p} = \frac{2 * \rho_{sub} * t_{sub}}{l_p * W_p} \quad , \quad R_{sub-p} = \frac{2 * \rho_{sub} * t_{sub}}{l_s * W_s} \tag{20}$$

Where, ρ_{cu}, ρ_{sub}: resistivity of conductor and substrate (ρ_{cu}=1,72 10^{-8} [Ωm], ρ_{sub} = 18,5 [Ωm]), t_{sub}, t_{ox}: thickness of substrate and SiO2 insulator (t_{sub} = 600 [µm], t_{ox} = 100 [µm]) , ε_{ox}, ε_{sub}: permittivity of SiO2 insulator and substrate ($\varepsilon_{r,ox}$ = 3,9 , $\varepsilon_{0,ox}$ = 8,85 10^{-12}[Fm^{-1}], ε_{sub} = 11,8).

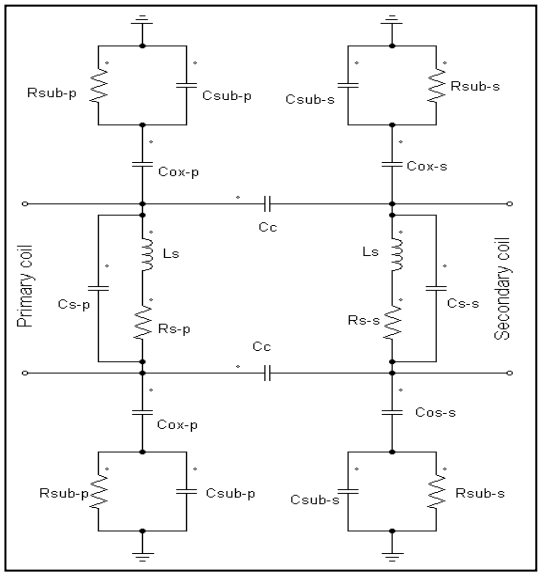

Figure 3: Model of the equivalent electrical circuit of spiral transformer.
Source: Authors, (2026).

The values of the electrical parameters of the integrated spiral transformer on silicon substrate are grouped in Table 2.

Table 2: Values electrical parameters of spiral transformer integrated.

Electrical parameters	Symbol	Values
Inductance series of primary coil	*Lp*	0,128 [µH]
Inductance series of secondary coil	*Ls*	0,226 [µH]
Resistance series of primary coil	*Rs-p*	0,1958 [Ω]
Resistance series of secondary coil	*Rs-s*	0,2829 [Ω]
Oxide capacitance of primary coil	*Cox-p*	4,4731 [pF]
Oxide capacitance of secondary coil	*Cox-s*	6,4612 [pF]
Substrate resistance of primary coil	*Rsub-p*	856,48 [Ω]
Substrate resistance of secondary coil	*Rsub-s*	592,94 [Ω]
Substrate capacitance of primary coil	*Csub-p*	2,2556 [pF]
Substrate capacitance of secondary coil	*Csub-s*	3,2582 [pF]
Capacitance series of primary coil	*Cs-p*	0,2882 [pF]
Capacitance series of secondary coil	*Cs-s*	1,2491 [pF]
Coupling capacitance between the primary and secondary coils	*Cc*	27,957 [pF]

Source: Authors, (2026).

IV.1 INTERPRETATION OF RESULTS

The objective of this study is to reduce energy losses within the transformer by addressing capacitive and resistive effects introducing parasitic currents. The calculated values of technological parameters, which are closely tied to geometric parameters, align seamlessly with the desired objectives. We notice that, they obtained results show particularly low values for the series resistances (*Rs-p* and *Rs-s*) of the primary and secondary coils. It is the same for the values of the inter-turn capacitances (*Cs-p* and *Cs-s*) and the capacitances (*Cox-p* and *Cox-s*) from the oxide layer. On the other hand, the substrate resistances (*Rsub-p* and *Rsub-s*) have high values, thus preventing the circulation of the low parasitic currents induced by the capacitive effect in the substrate. Figure 4 shows a simplified model of a micro transformer including two inductors, where the primary inductance and resistance are denoted by *Lp* and *Rp*, while the secondary inductance and resistance are denoted by *Ls* and *Rs*, as well as the coupling coefficient *k* and quality factors for the primary and secondary windings *Qp* and *Qs*.

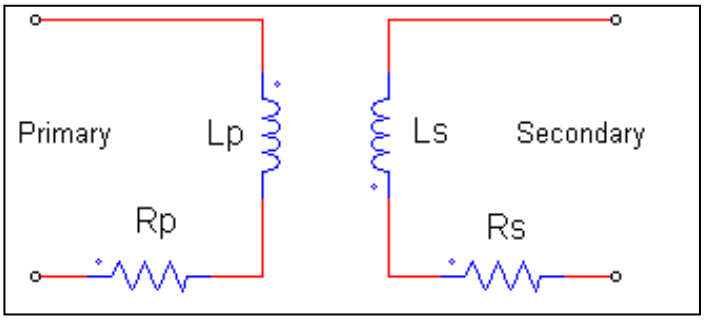

Figure 4: Simplified micro transformer model.
Source: Authors, (2026).

These elements, which represent the transformer specifications, are extracted from the Z-parameters, which are expressed as follows [22], [23]:

$$L_p = \frac{Im(Z_{11})}{2\pi f} \tag{21}$$

$$L_s = \frac{Im(Z_{22})}{2\pi f} \tag{22}$$

$$R_p = Re(Z_{11}) \tag{23}$$

$$R_s = Re(Z_{22}) \tag{24}$$

$$Q_p = \frac{Im(Z_{11})}{Re(Z_{11})} \tag{25}$$

$$Q_s = \frac{Im(Z_{22})}{Re(Z_{22})} \tag{26}$$

$$k = \sqrt{\frac{Im(Z_{12}) * Im(Z_{21})}{Im(Z_{11}) * Im(Z_{22})}} \quad 27)$$

V. SIMULATION AND RESULTANTS

V.1 INFLUENCE OF FREQUENCY ON THE INDUCTANCES OF THE PRIMARY AND SECONDARY

Based on relations (21) and (22) that were extracted from the imaginary part of the impedances, the variations of the primary and secondary inductances as a function of frequency were shown as shown in Figure 5. This figure gives a noticeable contrast between the primary and secondary inductors, which go through two stages: before the resonance frequency from 1 to 23 [MHz], the two inductors behave inductively, where the inductance values at a frequency of 5 MHz are 0,128 [µH] for the primary coil and 0,226 [µH] for the secondary coil, and with increasing frequency the inductances reach values climax at 20 [MHz]. But after the resonant frequency they behave capacitive.

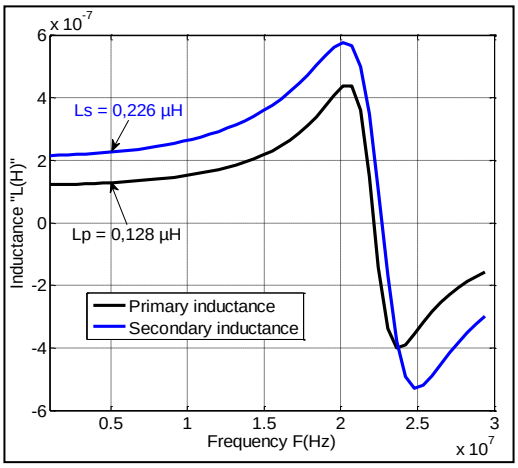

Figure 5: Variation of the primary and secondary inductances as a function of frequency.
Source: Authors, (2026).

V.2 INFLUENCE OF FREQUENCY ON THE SERIES RESISTANCES OF THE PRIMARY AND SECONDARY

Figure 6 depicts variation the series resistances of primary and secondary inductors as function of frequency, which was extracted from the real parts of the impedances according to two relations (23) and (24). At 5 [MHz], the resistances of the primary and secondary windings give low values of 0,195 [Ω] and 0,282 [Ω], respectively, due to the losses resulting from very low Joule effects. As the frequency increases, the series resistances of both windings begin to increase until they reach a peak at a frequency of 20 [MHz], which is known as resonance.

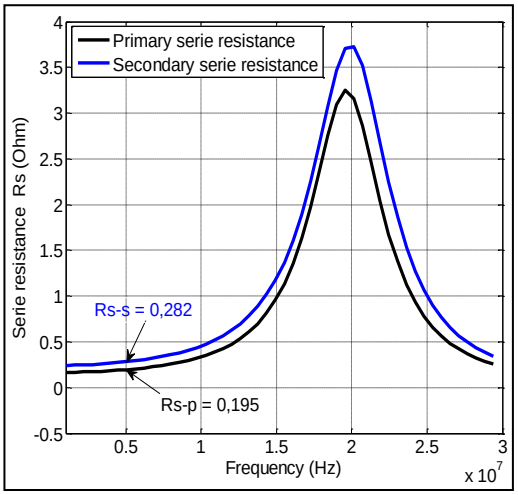

Figure 6: Variation of the primary and secondary series resistances as a function of frequency.
Source: Authors, (2026).

V.3 INFLUENCE OF FREQUENCY ON THE QUALITY FACTOR OF PRIMARY AND SECONDARY INDUCTANCES

Figure 7 shows the effect of frequency on variations in the quality factors of the primary and secondary inductors, which were previously expressed by relations (25) and (26) extracted from the real and imaginary parts of the impedances. In the first stage, it was observed that as the frequency increased, the quality factors increased until they reached the maximum values corresponding to the frequency of 13 [MHz], where the maximum value for the primary inductor is 25 and 20 for the secondary inductor. In the second stage, the quality factors decrease with increasing frequency until they reach zero, which is known as the resonant frequency point.

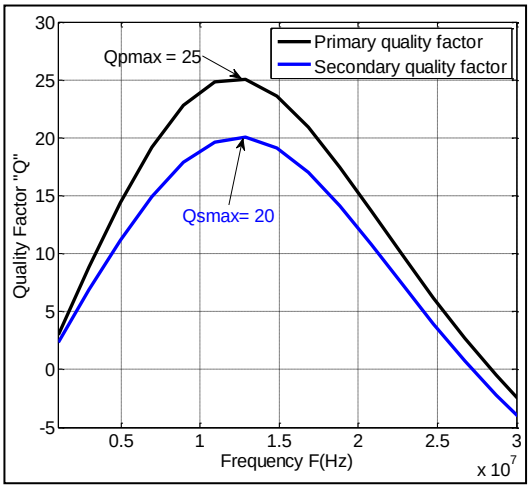

Figure 7: Variation of the primary and secondary quality factor as a function of frequency.
Source: Authors, (2026).

V.4 INFLUENCE OF FREQUENCY ON THE COUPLING COEFFICIENT

The curve shown in Figure 8 gives the evolution of the coupling coefficient between the two windings of the transformer as a function of frequency, which was previously expressed by relation (27) deduced from the imaginary parts of the impedances. We can notice that the coupling coefficient increases significantly at low frequencies, but after a frequency of 10 [MHz] this increase is very small until it reaches approximately 87 %.

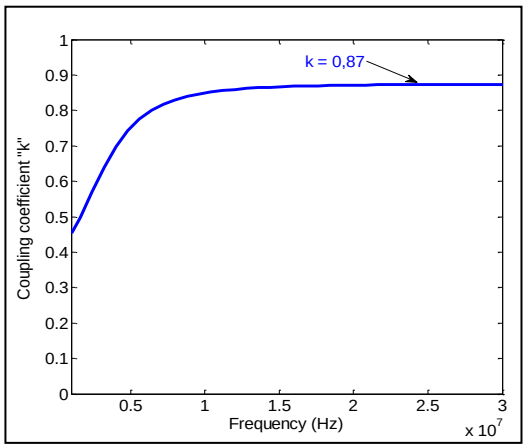

Figure 8: Evolution the coupling coefficient as a function of frequency.
Source: Authors, (2026).

V.5 SIMULATION OF INTERLEAVED FLYBACK CONVERTER WITH INTEGRATED SPIRAL TRANSFORMER IN PHOTOVOLTAIC SYSTEM

In this section, we simulate the operation of the photovoltaic system of interleaved flyback converter containing two spiral transformers using the PSIM program. This simulation aims to see the voltage and current graphs at the output of a DC/DC converter. Figure 9 shows a comprehensive diagram of the PV system at PSIM consisting of a solar panel, interleaved flyback converter with a integrated spiral transformers and the required load.

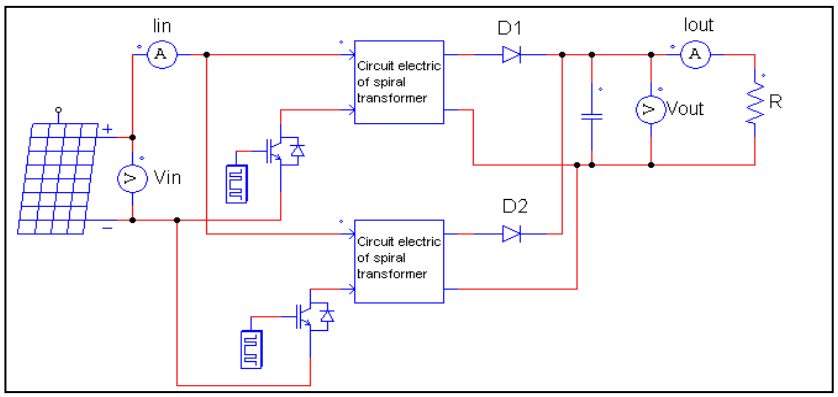

Figure 9: photovoltaic system consisting of interleaved flyback converter with integrated two spiral transformers.
Source: Authors, (2026).

Figures 10 show the current and power to voltage characteristics of the photovoltaic module with standard parameters (S = 1000 [W/m^2]. T = 25 [°C]). The maximum photovoltaic current reaches 6.75 [A] and the maximum power is about 153 [W] for a voltage of 24 [V].

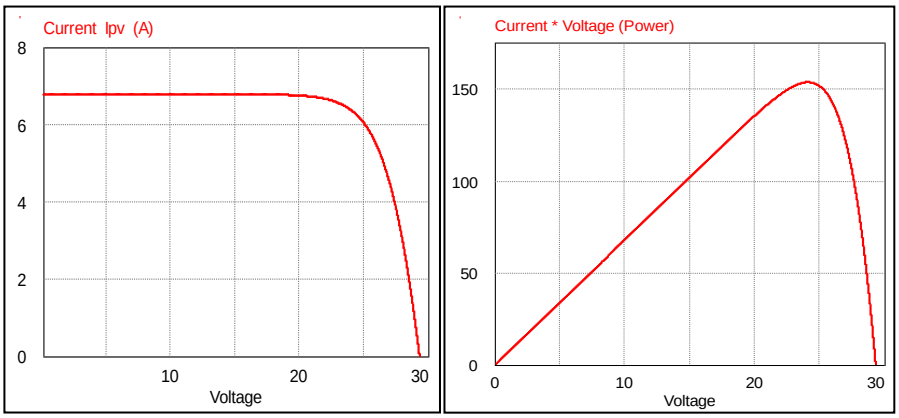

(a) **(b)**

Figure 10: Characteristics of the module photovoltaic, (a)current–voltage, (b) Power-voltage.
Source: Authors, (2026).

Figure 11 (a) show the output voltage form of interleaved flyback converter with integrating two spiral transformers stabilized at value 48 [V] starting from moment 6 [ms]. The value of the output current is about 3.2 [A] as shown in figure 11 (b), which indicates a stable and continuous transfer of power to the load.

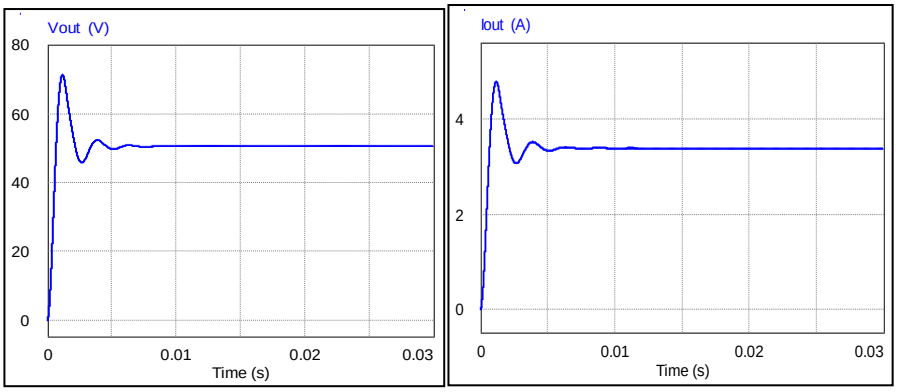

(a) **(b)**

Figure 11: (a) Output voltage and (b) Output current form of interleaved flyback converter with two spiral transformers integrated.
Source: Authors, (2026).

Since the interleaved flyback converter consists of two identical transformers connected in parallel and operating in alternating mode, simulation results for one of these transformers give the voltage and current for the primary and secondary windings, as shown in Figure 12.

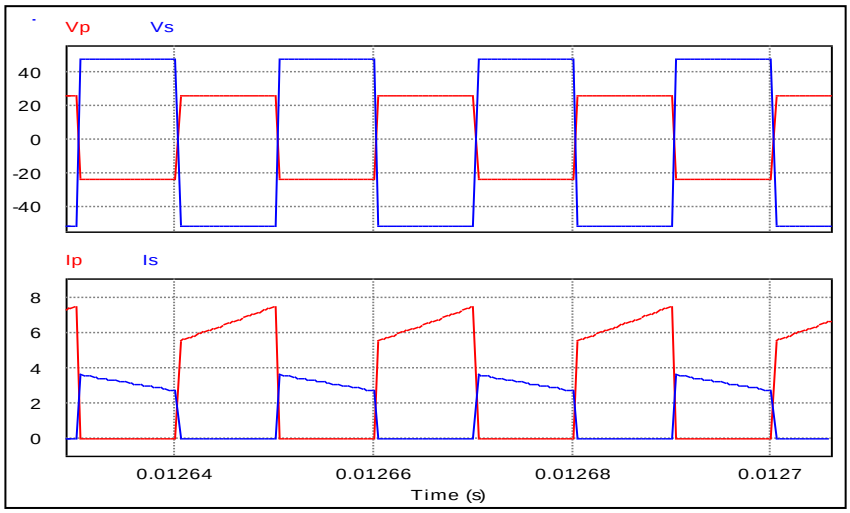

Figure 12: Voltage and current of the primary and secondary windings of the transformer integrated into the interleaved flyback converter.
Source: Authors, (2026).

VI. CONCLUSION

In the context of this study, we investigated the possibility of incorporating two spiral transformers within an interleaved Flyback converter specifically designed for photovoltaic applications. Our main goal is to reduce the dimensions of converters, fundamental components in photovoltaic systems, where the footprint in terms of size and weight poses a significant challenge. Reducing the dimensions of an interleaved Flyback converter necessarily involves decreasing the size of its transformers. In this regard, our work primarily focused on the miniaturization of coils. Initially, adhering rigorously to the converter specifications, we calculated crucial values of transformer parameters, including primary and secondary inductances, as well as the transformation ratio.

These parameters served as the basis for calculating all geometric parameters of primary and secondary coils (inner and outer diameters, conductor dimensions, number of turns, and inter-turn distance). The geometric sizing results were within integration standards. However, this step proved insufficient to ensure the proper functioning of the two transformers. So, it was imperative to precisely calculate the values of electrical parameters, responsible for various parasitic effects, to guarantee optimal operation. The obtained results reveal particularly low values for the series resistances (*Rs-p* and *Rs-s*) of the primary and secondary coils, as well as for inter-turn capacitances (*Cs-p* and *Cs-s*) and capacitances (*Cox-p* and *Cox-s*) resulting from the oxide layer.

On the other hand, substrate resistances (*Rsub-p* and *Rsub-s*) exhibit high values, providing significant resistance to the low parasitic current induced by capacitive effects in the substrate. Using the simplified electrical model of the transformer and the Z matrix, we expressed in detail the essential components of the transformer as a function of frequency. This approach allowed us to analyze the variation curves of primary and secondary inductances, *Ls* and *Lp*, with respect to frequency, as well as that of the series resistances, the quality factor *Q*, and the transformation ratio *k*. The results revealed a resonance frequency of 20 MHz, wich is quite high compared to the operating frequency (5 MHz).

However, at the operating frequency, the values of inductances and resistances indicated by the curves perfectly matched those obtained by calculation. The curves also highlighted satisfactory quality factors and a coupling coefficient of 0.87. Simulation results of the voltage and output current of the Flyback converter, incorporating the two dimensioned spiral transformers, were in accordance with the converter specifications. These results attest to the proper functioning of our converter. In conclusion, it is plausible to assert that the miniaturization of equipment in photovoltaic systems is entirely feasible.

VII. AUTHOR'S CONTRIBUTION

Conceptualization: Benzidane Mohammed Ridha, Namoune Abdelhadi.
Methodology: Benzidane Mohammed Ridha, Namoune Abdelhadi.
Investigation: Benzidane Mohammed Ridha, Namoune Abdelhadi, Benbouzid Zineb, Benyamina Mansour, Meskine Said.
Discussion of results: Benzidane Mohammed Ridha, Namoune Abdelhadi, Benbouzid Zineb, Benyamina Mansour, Meskine Said.
Writing – Original Draft: Benyamina Mansour, Meskine Said.
Writing – Review and Editing: Benzidane Mohammed Ridha, Namoune Abdelhadi, Benbouzid Zineb, Benyamina Mansour, Meskine Said.
Resources: Benzidane Mohammed Ridha,Benyamina Mansour, Meskine Said.
Supervision: Benzidane Mohammed Ridha, Namoune Abdelhadi, Meskine Said.
Approval of the final text: Benzidane Mohammed Ridha, Namoune Abdelhadi.

VIII. REFERENCES

[1] S. Zou, J. Lu, A. Mallik, and A. Khaligh, "Modeling and optimization of an integrated transformer for electric vehicle on-board charger applications," IEEE Trans. Transp. Electrif., vol. 4, no. 2, pp. 355-363, Jun. 2018.

[2] A. Namoune, R. Taleb, M. R. Benzidane, N. Mansour, H. Saidi, S. Tahraoui, and H. Houari, "Simulation study of the effects of different materials used in the core of a TSV inductor on its behavior when integrated into a DC/DC converter," Stud. Eng. Exact Sci., vol. 5, no. 2, pp. 11626-11626, Jul. 2024.

[3] R. Melati, M. R. Benzidane, V. Bley, and T. A. Benattia, "Design, modeling, and fabrication of an ultra-thin planar capacitor," J. Electron. Mater., vol. 53, no. 1, pp. 449-461, Jan. 2024.

[4] M. R. Benzidane, R. Melati, M. Benyamina, S. Meskine, P. Spiteri, A. Boukortt, and T. A. Benattia, "Miniaturization and optimization of a DC–DC boost converter for photovoltaic application by designing an integrated dual-layer inductor model," Trans. Electr. Electron. Mater., vol. 23, no. 5, pp. 462-475, Oct. 2022.

[5] A. Namoune, R. Taleb, and M. R. Benzidane, "Design and simulation of integrated spiral inductor a boost converter for photovoltaic application," Ing. Energ., vol. 44, no. 1, pp. 01-12, Jan. 2023.

[6] Y. Cao, K. Ngo, and D. Dong, "A scalable electronic-embedded transformer, a new concept toward ultra-high-frequency high-power transformer in DC–DC converters," IEEE Trans. Power Electron., vol. 38, no. 8, pp. 9278-9293, Aug. 2023.

[7] N. Abdelhadi, B. M. Ridha, M. Rabia, B. Abdelkader, A. B. Tekkouk, and B. Zineb, "Integrated interleaved transformer in an isolated full-bridge buck converter," J. Circuits Syst. Comput., vol. 33, no. 9, pp. 2450168-2450168, May 2024.

[8] T. A. Benattia, R. Melati, H. L. Beklaouz, H. Azzedine, V. Bley, C. Combettes, and M. R. Benzidane, "Dimensioning and realization of an LTCC multilayer capacitor for energy conversion," Trans. Electr. Electron. Mater., vol. 21, no. 5, pp. 564-579, Oct. 2020.

[9] A. Namoune, A. Hamid, and R. Taleb, "The performance of an integrated transformer in a DC/DC converter," TELKOMNIKA Telecommun. Comput. Electron. Control, vol. 15, no. 3, pp. 1031-1039, Sep. 2017.

[10] M. A. Taha, D. A. Oumar, A. Abderahim, S. Capraro, D. Pietroy, J. P. Chatelon, and J. J. Rousseau, "Simulation, modeling, manufacturing, and characterization of a planar magnetic face to face integrated transformer," IEEE Trans. Magn., vol. 54, no. 12, pp. 01-12, Dec. 2018.

[11] A. Namoune, R. Melati, M. R. Benzidane, S. Pierre, and B. Abdelkader, “Substrate thickness effect on the integrated interleaved transformer in RF,” UPB Sci. Bull. Ser. C, vol. 85, no. 3, pp. 377-392, Jul. 2023.

[12] R. Bajwa and M. K. Yapici, “Integrated on-chip transformers: Recent progress in the design, layout, modeling and fabrication,” Sensors, vol. 19, no. 16, pp. 3535-3535, Aug. 2019.

[13] F. Tounsi, D. Flandre, L. Rufer, and L. A. Francis, “Performances evaluation of on-chip large-size-tapped transformer for MEMS applications,” IEEE Trans. Instrum. Meas., vol. 69, no. 9, pp. 7051-7060, Sep. 2020.

[14] A. Namoune, M. R. Benzidane, R. Taleb, A. Boukortt, Z. Benbouzid, and M. Benyamina, “Design and simulation of a high-efficiency micro-transformer for photovoltaic application,” Electr. Power Compon. Syst., vol. 52, no. 17, pp. 01-17, Jul. 2024.

[15] A. Namoune, R. Taleb, N. Mansour, M. R. Benzidane, and A. Boukortt, “Integrated through-silicon-via-based inductor design in buck converter for improved efficiency,” Electr. Eng. Electromech., no. 6, pp. 54-57, Nov. 2023.

[16] C. Chen, P. Pan, D. Lyu, J. Gu, M. Liu, and X. Li, “Wafer-level fabricated tight-coupling dual-solenoid transformer chips with watt-scale power transfer,” IEEE Trans. Power Electron., vol. 38, no. 4, pp. 5118-5127, Apr. 2023.

[17] K. Zhu, H. Chen, S. Li, C. Sun, and F. Liu, “An RF on-chip transformer with Fe3O4/GO nano-composite film,” IEEE Trans. Magn., vol. 57, no. 2, pp. 01-08, Feb. 2021.

[18] Z. Zhang, K. Xu, Z.-W. Xu, J. Xu, X. Ren, and Q. Chen, “GaN VHF converters with integrated air-core transformers,” IEEE Trans. Power Electron., vol. 34, no. 4, pp. 3504-3515, Apr. 2019.

[19] A. Venugopal and F. Robert, “Analysis of a non-overlapping interleaved planar transformer winding structure with reduced parasitic effects,” Iran. J. Sci. Technol. Trans. Electr. Eng., vol. 46, no. 3, pp. 689-700, Sep. 2022.

[20] H. Li, K. Zhu, K. Lei, T. Xu, and H. Wu, “Integrated MEMS toroidal transformer with Ni-Zn ferrite core for power supply on chip,” IEEE Trans. Power Electron., vol. 37, no. 9, pp. 10075-10080, Sep. 2022.

[21] M. Cheng, L. Liu, Z. Liao, J. Yu, S. Peng, Z. Zhang, T. G. Ye, and N. Wang, “On silicon-integrated micro-transformers and their applications in quasi-resonant flyback converters,” IEEE Trans. Magn., vol. 58, no. 6, pp. 01-12, Jun. 2022.

[22] A. Namoune, A. Hamid, and R. Taleb, “Stacked transformer: influence of the geometrical and technological parameters,” Int. J. Eng. Res. Afr., vol. 21, pp. 148-164, Feb. 2016.

[23] A. Namoune, A. Hamid, and R. Taleb, “Simulation analysis of geometrical parameters of monolithic on-chip transformers on silicon substrates,” Przegl. Elektrotech., vol. 93, no. 1, pp. 253-257, Jan. 2017.